REDVET - Revista electrónica de Veterinaria - ISSN 1695-7504
Vol 25, No. 1 (2024)
http://www.veterinaria.org
Article Received: 12 Jan 2024, Revised: 28 Jan 2024, Accepted: 16 Feb 2024

MOHO DEPTH UNDULATIONS BELOW THE BAY OF BENGAL USING 3D INVERSION OF GRAVITY DATA

Srinivasarao Manchala[1]*, S.K. Begum Priyesh Kunnummal[2]

[1*]Department of Geophysics, Andhra University, Visakhapatnam-530003, Andhra Pradesh, India
[2]Indian Institute of Geomagnetism, Navy Mumbai, Maharashtra 410218, India

***Corresponding author:** Srinivasarao Manchala
*Email:manchalasrinu423@gmail.com

Abstract:
A high-resolution satellite-derived free air gravity data set has been used in the Bay of Bengal. Bullard A (Bouguer plate), Bullard B (Curvature), and Bullard C (Terrain) corrections were applied to the Indian Geoidal Low derived from the Free Air gravity data (often referred to as FAG-IOGL) data in order to create a Complete Bouguer Anomaly (CBA). The Parker Method was first employed in order to invert the CBA data and generate Moho topography. From the CBA data, the Mantle Residual Gravity Anomaly (MRGA) has been derived by removing the gravitational impacts, lithosphere- and pressure-induced anomalies created by the sediments. Moreover, the Moho undulations were produced by inverting the MRGA, and these have been used for calculating the Crustal thickness. Moho depths estimated with the MRGA and CBA are, respectively, 13 to 30 km and 10 to 26 km. The range of predicted crustal thickness is 2–28 km. Moho depths, as determined by CBA and MRGA, are shallower in the western basin between latitudes 7˚N and 15˚N, or in the direction of the 85˚E Ridge on both the western and eastern sides. However, the lowest Moho (i.e., 25 and 23 km from the CBA & MRGA) is found at latitude 14˚N underneath the 85˚E Ridge. Deeper Moho depths of 21 and 23 km are derived from the CBA and MRGA beneath 90˚East Ridge, at the southern end of the research area. In our study area, the sediment thickness increases from 1000 m at the southernmost spot to 11,000 m at the northernmost spot. In the area under study, the bathymetry fluctuates from 500 m north to 4500 m south. The thickness of the crust has increased to 8–12 km below the 85°E Ridge, but it has decreased to 2–4 km on both of the ridge's boundaries. At the extreme SSE BoB, the crustal thickness is 19 km.

Key words: 85˚E Ridge, 90˚East Ridge, Moho undulations, Free Air Gravity Anomaly, 3D gravity inversion. Crustal thickness.

1. INTRODUCTION:

When Australia-Antarctica and Greater India split into two separate continental masses throughout the Early Cretaceous, the eastern Indian Ocean started to evolve (Curray et al., 1982; Powell et al., 1988; Lawver et al., 1991; GopalaRao et al., 1997; Gaina et al., 2003, 2007). In the Eastern Indian Ocean, seafloor spreading occurred in three stages: first, it drifted in a NW-SE direction until the middle of the Cretaceous period; second, it drifted in an N-S direction until the early Tertiary period; and third, it proceeded in a NE-SW direction. When India first collided with the subduction zone on the north side of the Tethys Ocean during the Palaeocene and Eocene, the Bay of Bengal formed (Curray & Moore, 1974; Curray, Emmel, Moore, & Raitt. 1982; Lee & Lawver, 1995; Alam, Alam, Curray, Choudhuri, & Gaina, 2003). Seismic ridges are a collection of topographically elevated, non-spreading, linear landforms on the seafloor that are created by rifting and uplift brought on by tectonic activity or by volcanic eruptions along leaky transform faults or hotspots. Before the impact, there was a thick continental rise prism of silt collected off the eastern border of India (Mukhopadhyay et al., 2008).Seismic ridges are an assortment of topographically brought up, erect, and non-spreading landforms on the seafloor that have been created by volcanic eruptions along leaky transform faults or hotspots, or by rifting and uplift resulting from tectonic activity.

A thick continental rise prism of silt gathered off the eastern border of India existed prior to the impact (Mukhopadhyay et al., 2008). There is a total of 3.5 km of silt covering the 85°E Ridge, which Curray et al. (1982) characterised as a subsurface foundation rise along the 85°E longitude. Many theories, including the following ones, have been put forth. The abandoned spreading centre (Mishra, 1991); the Hotspot Volcanic Chain (Curray and Munasinghe, 1991; Muller, 1993; GopalaRao et al., 1997); the Lithospheric Flexure (Liu et al., 1982); the Sagging of the Crust (Shemenda, 1992); and even an intra-plate deformation as a result of the Indian-Eurasian collision (Anand et al., 2009). Despite the fact that several researchers have concluded that the two magmatic and tectonic processes helped to the formation of the 85°East Ridge during the Mesozoic North ward drift of the Indian plate, Chaubey et al., 1991; Curray and Munasinghe, 1991; Kent et al., 1992; Krishna, 2003; Anand et al., 2009; Bastia et al., 2010; Desa et al., 2013; Krishna et al., 2014; Srinivasarao and Radhakrishna, 2014; Choudhuri et al., 2014, 2017; Ismaiel et al., 2017).The 90°E meridian will be followed by the Ninety East Ridge, which covers from 34°S to 17°N latitudes with a typically N-S trend.

REDVET - Revista electrónica de Veterinaria - ISSN 1695-7504
Vol 25, No. 1 (2024)
http://www.veterinaria.org
Article Received: 12 Jan 2024, Revised: 28 Jan 2024, Accepted: 16 Feb 2024

With dimensions of around 5600 km in length, 200 km in width, and 2000 km in height, it is the longest linear aseismic linear feature on Earth. According to Weis et al., 1991; Ramana et al., 2001 (references therein), the Kerguelen hotspot has confirmed that the Ridge is an emplacement (Yatheesh. 2020). Krishna et al. (2012) estimated that the length of the Ninety East Ridge is twice that of the neighbouring oceanic crust based on a comparison of the ages of the oceanic crust east and west of the Ridge and the radiometric ages of the DSDP and ODP sites. Between the Nicobar Fan and the Bengal Fan to the west, the Ninety East Ridge is composed of a complex network of echelon blocks that are located off the Sunda subduction zone (Curray and Moore, 1974; Sclater and Fisher, 1974).

Given that some researchers believe continental crust or continental, many years of marine geophysical study in the Bay of Bengal have been carried out to gain a better understanding of the composition and structure of the crust (Krishna, 2003; Sarma et al., 2002; Subrahmanyam et al., 1999, 2001; Ramana et al., 2001 and references therein). It is imperative, Sliver, to identify the precise composition of the crust underneath every ridge. This work assesses the Moho depth and the variances in crustal thickness beneath the Bay of Bengal, including the Central Indian Basin and the surrounding area, the 85°East Ridge, and the 90°East Ridge, in an attempt to better understand the nature of the crust.

High resolution satellite-derived free air gravity data serves as the foundation for these evaluations. This is accomplished by incorporating the sediment gravity corrections, the temperature and pressure corrections for the Lithospheric region, and inverted the Mantle Residual Gravity Anomaly and Complete Bouguer Anomaly. This has made it possible for the calculation of Moho undulations and crustal thickness beneath the Bay of Bengal. Understanding the depths and crustal thickness underneath the 85º East and 90º East Ridges and the region surrounding them to the Moho interface is the key objective of the current study. The Bay of Bengal's free air gravity map that was created as a result of this study is shown in Figure 1. Schematic map of the study area, Bay of Bengal has been shown in the Figure 2.

2. Geology and Geomorphology

Younger oceanic crust produced by the N-S moving seafloor spreading beneath the eastern portions of the Bay of Bengal is depicted by the E-W trending magnetic lineation. Older oceanic crust was produced by seafloor spreading going NW-SE prior to 100 Ma plate reorganisation. The Eastern Continental Margin of India (ECMI) is parallel to a magnetic lineation that trends from N-S to NE-SW, and this lineation dominates the northwest section of the Bay of Bengal. The direction of plate reorganisation and seafloor spreading has changed over the last 100 million years. Despite the oceanic crust beneath the Bay of Bengal is of this type, there is disagreement on how old it is. A study conducted by Ramana et al. (1994) investigated the possibility that M-series anomalies in the Bay of Bengal linked to a moderate crustal stretch could explain the Cretaceous Magnetic Quiet Era (120-80 Ma). India and Antarctica split approximately 120 Ma, according to another study (GopalaRao et al., 1997). Krishna and GopalaRao (1997) then conjectured that the oceanic crust under the Bay of Bengal might include relics of past spreading centres and transported Antarctic plate crust, with the latter event occurring between 90 and 95 Ma. Based on the minimum age of the oceanic crust in the Bay of Bengal (~120 million years), Shorshchikov et al. (1995) clarify that that the 85°East Ridge on the Lithosphere has been formed by a hot spot that was at least 35 million years older than the hot spot.

According to Shorshchikov et al. (1995), the minimum age of the oceanic crust in the Bay of Bengal (~120 million years) points to a hot spot that was at least 35 million years older than the hot spot developed the 85°East Ridge on the Lithosphere. Numerous scholars have linked a hot spot or plume to the creation of the 85°E Ridge (Bastia et al., 2010; Curray and Munasinghe, 1991; GopalaRao et al., 1997; Muller et al., 1993). According to SrinivasaRao and Radhakrishna (2014), the Conrad mantle plume generated the southernmost portion of the 85°E Ridge, whereas the Kerguelen mantle plume developed the growth of the northernmost portion of the Ridge using magmatic material. The north leg of the 85°E Ridge erupted along a pseudo fault surrounding the middle of the Cretaceous epoch, partly due to melting produced by the Kerguelen mantle plume (Desa et al. 2013). Ninety East Ridge (NER) is another noteworthy aseismic ridge within the current investigation region. Sclater and Fisher (1974) discovered three morphologically distinct domains underneath NER: the narrow, linear, and discontinuous central domain is located south of 5°S to Osborn Knoll (NER's western side); the wider, somewhat less linear southern domain is located south of Osborn Knoll. The wide ridge in the northern domain is made up of irregularly shaped blocks.

3. Morpho-tectonic elements and previous studies

These ridges offer substantial relief beneath the Bay of Bengal, the Sunda Arc system, the passive continental edge of India, and north-south trending aseismic ridges like the 85º and 90º East Ridges. These are the most prominent morph tectonic elements in the research area. The development of the buried 85°East Ridge may have occurred during one of the reversals that occurred during the Middle Cretaceous era, based on integrated study by Ramana et al. (1997b, 2001). The start of the volcanism in this Ridge is thought to have been brought about by a short-lived hot spot that caused anomaly 33r time (~80 Ma) in the Mahanadi Basin. Following that, the procedure proceeded southward till it ended near the Afanasy Nikitin Seamount. This ridge exhibits different gravitational and magnetic signatures: a northward-facing negative anomaly up to 5ºN is correlated with the ridge, and a southward-facing positive anomaly. Ridge, on the other

hand, reveals positive and negative alternating bands with asymmetrically distributed magnetic signatures (Michael, L. and Krishna, K.S., 2011).In accordance with Michael L. and that Krishna, K.S. (2011), the seamount has an age of 55 Ma.

The 85ºE Ridge has been associated with a negative gravity anomaly (Liu et al., 1982). Several studies (Weis and Frey, 1991; Weis et al., 1991; Klootwijk et al., 1992; Duncan, 1991; Duncan and Storey, 1992) have proven that Ninety East Ridge (NER), a major, The longest feature on Earth, known as NER, follows the 90ºE meridian and spans nearly 5000 km, or between 30ºS and 17ºS. Seismic and bathymetric studies have revealed that NER has irregular borders, an average width of 200 km, and relief greater than 2 km (Sclater and Fisher, 1974; Fisher et al., 1982; Krishna et al., 1995, 2001a; Sager et al., 2013). The Age of the Ridges has risen from north to south (77 Ma at ODP Site 758), as determined by geochronological examinations of core samples from the Ocean Drilling Programme (ODP) Sites 758, 756, and the Deep Sea Drilling Project (DSDP) Sites 216, 214, and 254 along the Northeast Ridge Expedition (NER) (Pringle and others, 2008).The BoB has been split into two deep sea sedimentary basins by the aseismic linear feature NER. They are listed in the following order: i)

Bengal Fan, the world's largest underwater fan, is situated west of the Ninety East Ridge. BoB is distinctive in that it spans 3000 km from 20°N to 7°40'S, making it unique(Curray et al. 2003; Krishna et al. 2001a). ii) Nicobar Fan is positioned to the east of the Ridge's ninety-east. The Bengal Fan has been separated into two additional basins by the 85°East Ridge. i) The Central Basin is situated at 85° and 90°, between the East Ridges. (Rao and BhaskaraRao, 1986). Many characteristics have been used to define the northern region of the Central Indian Basin: the former spreading ridge segments, the NS veering fracture zones, the EW trending magnetic lineation, and the former spreading ridge segments (Schlich, 1982; Norton and Sclater, 1979; Liu et al., 1983; Royer et al., 1989; Krishna et al., 1995, 1998). ii) The Indian Western Basin, which extends from the 85° East Ridge to the eastern continental shelf (Curray et al., 1982, Rao et al., 1994; Rao and Rao, 1986). In the words of Baksi et al. (1987), Sylhet traps originated in the Mahanadi Basin about 107 Ma, while Rajmahal traps evolved from the Kerguelen hot spot about 118 Ma.

Bengal Basin is home to the Rajmahal traps. There are in fact three parts to the Bengal Fan. These are: i) Upper Fan, off Ganges delta, carrying the Swatch of No Ground's southern extension. ii) Lower Fan; iii) Middle Fan. Bengal Fan offered the complete early evolutionary history of the Andaman Group of Islands in the east, the north and east coasts of the Burma Plateau, and the north eastern Indian Ocean (Curray and Moore, 1974).

4. Qualitative analysis from Geoid corrected FAG and CBA maps

4.1 Geoid corrected FAG map: With an amplitude ranging from about -180 mGal to 300 mGal, the primary wavelength anomalies on this map (Figure 4) are shallow to moderate.

The N-S trending gravity low anomalies were utilised to identify the 85°East Ridge. In comparison with the surrounding ocean floor, which exhibits larger amplitudes, the anomaly above the 85°East Ridge is rather minor. But there's no view of Ninety East Ridge. The 85°East Ridge is linked to a gravity low anomaly that is trending northward. With an amplitude ranging from -20 mGal to -40 mGal, the appropriately substantial gravity anomaly borders the gravity low anomaly and is located over the 85°East Ridge between latitudes 13°N and 15°N. The 20 mGal contour, showing the N-S trending shallow wavelength gravity closure with amplitude from 20 mGal to 40 mGal, borders the relatively low gravity anomaly with an amplitude ranging from -20 mGal to +20 mGal towards the eastern flank of the 85°East Ridge in the western basin, between 12°N and 15°N. A few decreasing wavelength minor gravity closures can be visible along the 85°East Ridge, in the western basin, between 12°N and 15°N, as one moves south of 15°N. The amplitude of -20 mGal contours the gravity anomaly, whose amplitude varies from 20 to 60 mGal. The amplitude range of the gravity anomaly, which is between -20 and -40 mGal, almost entirely encompasses the central basin.

In the Central Basin, little low gravity closures are seen south of 10°N. The relatively high gravity anomaly inhibited the NE-SW trending gravity low anomaly, whose amplitude ranged from -40 mGal to -20 mGal, between latitudes 14.5°N and 15.5°N. The amplitude -20mGal contour defines this low gravity closure. The 20mGal contour, having an amplitude range of 20mGal to 60mGal, reflects the NE-WWS trending gravity anomaly of the Central Basin between latitudes 11°N and 13°N, west of the Sunda arc trench. With an amplitude ranging from -20 to 20 mGal, a rather minor gravitational anomaly surrounds it. West of the Sunda arc trench and south of latitude 12°N, in the lower Fan, is a NW-S trending gravity anomaly with an amplitude ranging from 20 to 60 mGal. It is encircled by a relative gravity low anomaly with amplitude that varies from -20mGal to 20mGal. North of 16°N, the Upper Fan exhibits a significant wave length gravity anomaly that is moving from -60mGal to -20mGal. A -20mGal contour encompasses the moderately substantial gravity anomaly, whose amplitude varies from -20mGal to +20mGal. An intermediate wavelength low gravity closure with a NE-SW trend is highlighted with a contour with an amplitude of -20mGal, situated off the Eastern Continental Margin of India between latitudes 16°N and 19.5°N.

REDVET - Revista electrónica de Veterinaria - ISSN 1695-7504
Vol 25, No. 1 (2024)
http://www.veterinaria.org
Article Received: 12 Jan 2024, Revised: 28 Jan 2024, Accepted: 16 Feb 2024

4.2 CBA map

The Complete Bouguer Anomaly (CBA) map (Figure 5) is dominated by N-S trending long wave length anomalies with amplitude ranges of -120mGal to +360Gal. This map was created by combining the FAG-IOGL (Figure 3) map with the Bouguer Plate (Bullard A), Curvature (Bullard B), Terrain (Bullard C) and Bathymetry corrections.

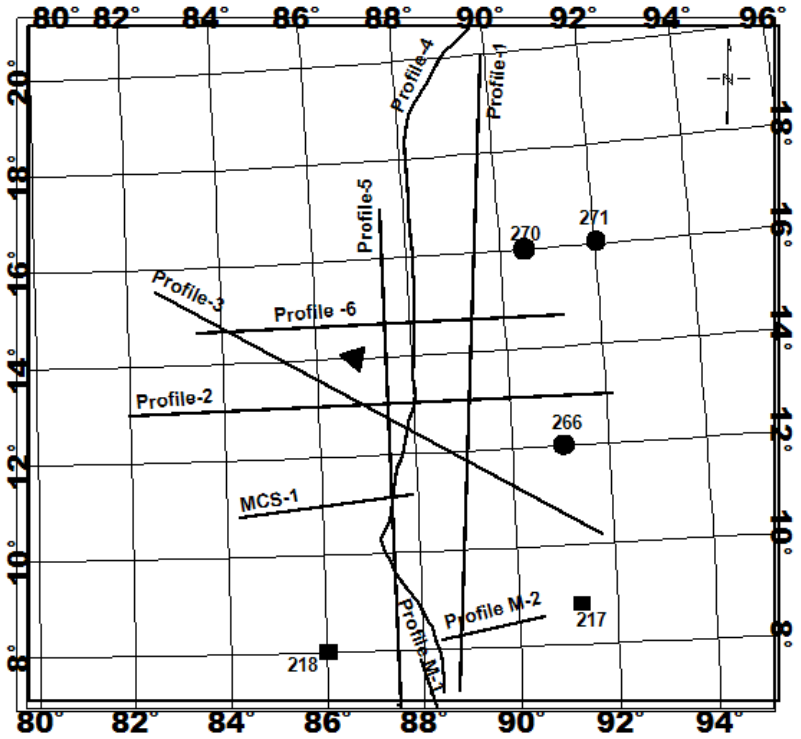

Figure 2: Bay of Bengal schematic map for the study region. The position of the DSDP 217 and DSDP 218 wells is shown by a solid box (Vonder Borch et al., 1977); the seismic refraction stations 266, 270, and 271 are indicated by solid circles (Naini and Layden.1973). Station for seismic refraction is shown by a solid triangle (Curray et al., 1982). Profile MCS-1 is derived from L. Shang et al 2022.'s seismic reflection investigations. 2. Profile-1 is taken from Corchete's 3DS-velocity research. 2017 Profiles 2 through 6 are taken from 2D geoid-gravity model research by G.S. Rao et al. (2016); Profiles 2 through 4 are taken from 3D gravity inversion investigations by Radhakrishna et al. (2010). Profiles M-1 (Mezen-1)

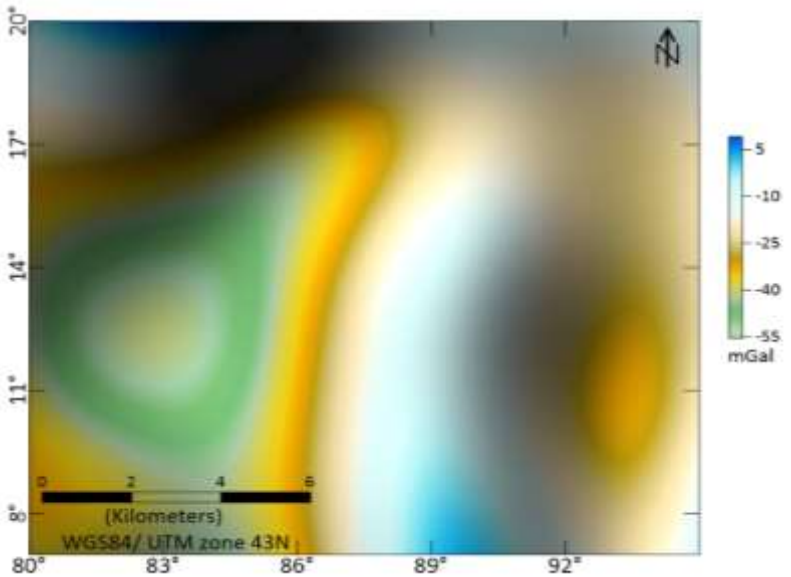

Figure 3: The Bay of Bengal's Indian Ocean Geoidal Low (IOGL) Free Gravity Map. Using the simple harmonic coefficients of EIGEN-6C4 up to order 50, the long wavelength gravity influence of the Indian Ocean Geoidal Low (IOGL) has been estimated and subtracted from the Free Air Gravity Anomaly (V.24.1, Sandwell and Smith, 2009)

REDVET - Revista electrónica de Veterinaria - ISSN 1695-7504
Vol 25, No. 1 (2024)
http://www.veterinaria.org
Article Received: 12 Jan 2024, Revised: 28 Jan 2024, Accepted: 16 Feb 2024

The 0 mGal anomaly contour surrounds N-S trending long wave length high gravity anomalies that are found in the Western Basin and the Central Basin between latitudes 15.5°N and 7°N, with the exception of a few N-S trending moderate gravity closures with an amplitude ranging from 300 to 360 mGal. The Central Basin lies between latitudes of around 18.5°N and 12°N. It is dominated by anomalies at long wavelengths with amplitudes ranging from 180 mGal to 240 mGal, running NNE-S. The contours at +180 mGal and 0 mGal, north and south of 16°N, are connected to this anomaly. A comparatively moderate gravity anomaly with an amplitude of 240mGal to 300mGal in the southernmost part of the Bay of Bengal, between latitudes 9°N and 7°N, defines the biggest N-S trending gravity anomaly, which is related to the 0mGal contour and ranges from 300mGal to 360mGal. In the northernmost part of the Bay of Bengal, between latitudes roughly 17°N and 19.5°N, there is a N-S trending long wave length gravity anomaly with an amplitude of 120–180 mGal that is boarded with a relatively low anomaly towards the north of 18°N and a relatively high anomaly towards the south of the 18°N latitude. The amplitude range of the gravitational anomaly increases towards the south of the 20°N line, which separates the latitudes of 20°N and 8°N. Similarly, the wave length's magnitude increases as one moves north of the 8°N latitude and between those latitudes. The size of the outlines rises and then falls. Central India and the western Basin exhibit the similar Bouguer anomalies. The southern section of the western and central Indian basins exhibits anomalies with a mass between 240 and 360 mGal. This pair of basins have an outside limit of 0 mGal and are encircled by a rather low Bouguer anomaly of 180–240 mGal.

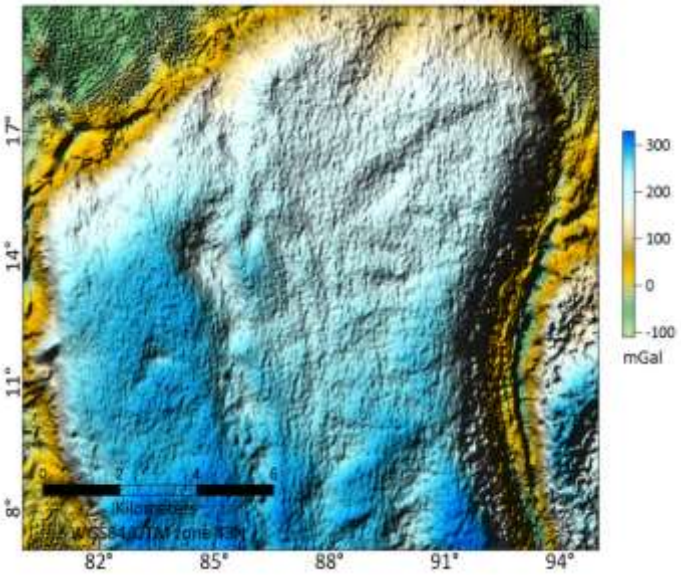

Figure 5: After applying Bouguer plate, curvature, and terrain correction to Geoid corrected FAG data, the complete Bouguer anomaly (CBA) map is produced. Densities of 2900 kg $^{-3}$and 1030 kg^{-3} were assumed for crust and seawater, respectively.

To begin with, Moho undulations were created by inverting CBA, which spared corrections for sediment, pressure, and lithospheric temperature. Moho undulations can be only possible when mean Moho depth, density contrast, and inversion of gravity were combined. Assumptions for the first iteration include a density contrast of 400 kgm^{-3} and a mean Moho depth of 21 km from Crust 1.0 (Laske et al., 2013). Because oceanic crust covers the research region, densities of 3300 kgm^{-3} for the mantle and 2900 kgm^{-3} for the crust have been assumed. After nine iterations, the inversion reached convergence. Figure 6 depicts the Moho undulations, which are inverted from the CBA and indicate the Moho depth beneath the 85° East Ridge, ranging from 18 to 24 Km. It is clear that, inside the ocean basin, Moho (13 km) is getting shallower on both sides of this ridge. The sediment thickness of all the world's seas, as recorded in Version 2 of the data set by Whittaker et al. (2013) and Divins (2003), provided by NOAA/NGDC, has been utilised to determine the gravitational anomalies generated by the layers of sediment. The sediment thickness model has an average horizontal dimension of 5.5 km and an average vertical resolution of 50 m. A map of sediment thickness is shown in Figure 7, using equation (1) and, the sediment density for each grid of the model has been determined. The ODP well 217 provided the porosity values (Figure 2). Since the current research area's average depth and the well's (5 km) average depth are same. Figure 8 shows the bathymetry map of the region under inquiry. Moreover, the age of these ocean floor cores, which is 50 million years old, corresponding to the average age of the ocean floor in the research area. Figure 9 displays the current study area's age. Figure 10 displays an exponential fit to the porosity versus depth plot. The plot demonstrates that the initial porosity is 0.7278 and the constant c has a value of 10.6×10−4/m. The porosity values at different depths (z) are computed using equation (1). Using the equation (2), the densities of the various sedimentary column layers have been calculated. Average measurements of the grain density from DSDP well 217 well are used to estimate the density of the pore fluid to be 1030 kgm^{-3} and the grain density to be 2700 kgm^{-3} (Vonder Botch et al., 1974). The estimated density

REDVET - Revista electrónica de Veterinaria - ISSN 1695-7504
Vol 25, No. 1 (2024)
http://www.veterinaria.org
Article Received: 12 Jan 2024, Revised: 28 Jan 2024, Accepted: 16 Feb 2024

estimates have been used to establish the overall gravitational influence caused by sediments; the value of this effect varies between about 20 mGal and 110 mGal.

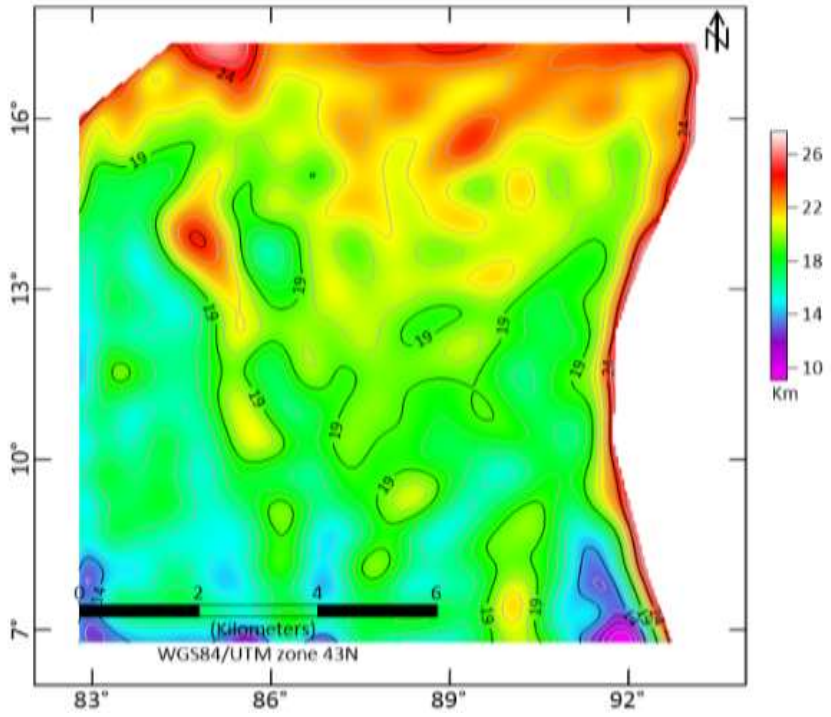

Figure 6: Moho Depths obtained from the 3D invereted Complete Bouguer Anomaly(CBA) Data without sediment,Temperature and Pressure corrections.

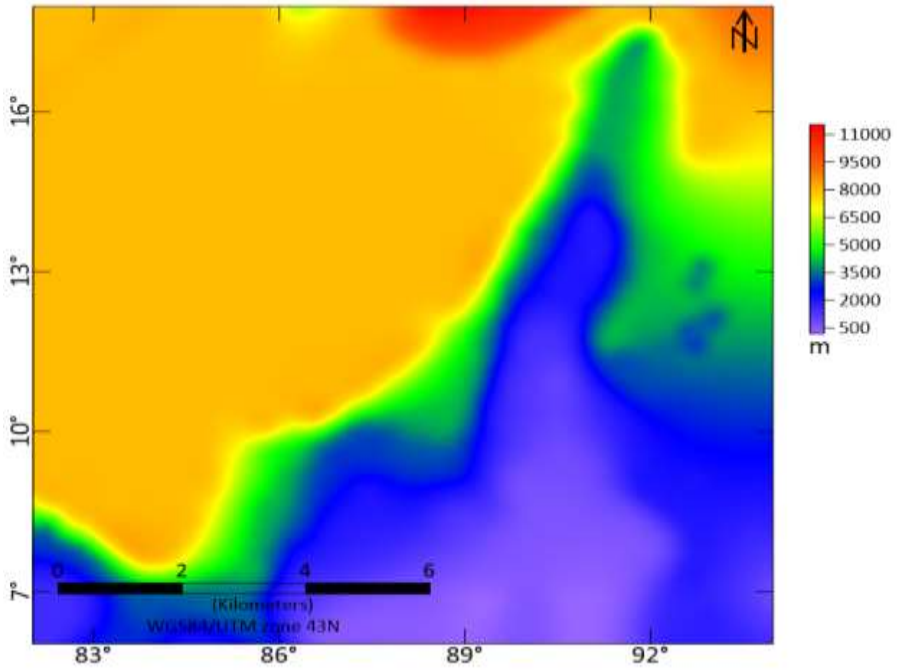

Figure 7: Sediment thickness map in the Bay of Bengal, after applying sediment correction to CBA

REDVET - Revista electrónica de Veterinaria - ISSN 1695-7504
Vol 25, No. 1 (2024)
http://www.veterinaria.org
Article Received: 12 Jan 2024, Revised: 28 Jan 2024, Accepted: 16 Feb 2024

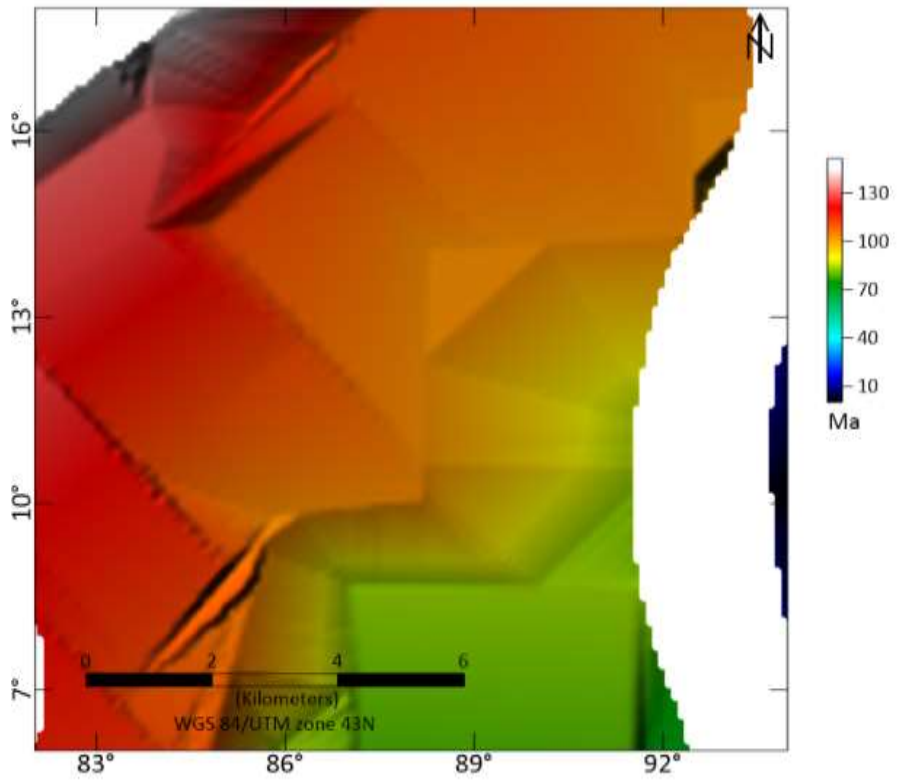

Figure 8: Map showing the Bathymetry in the Bay of Bengal

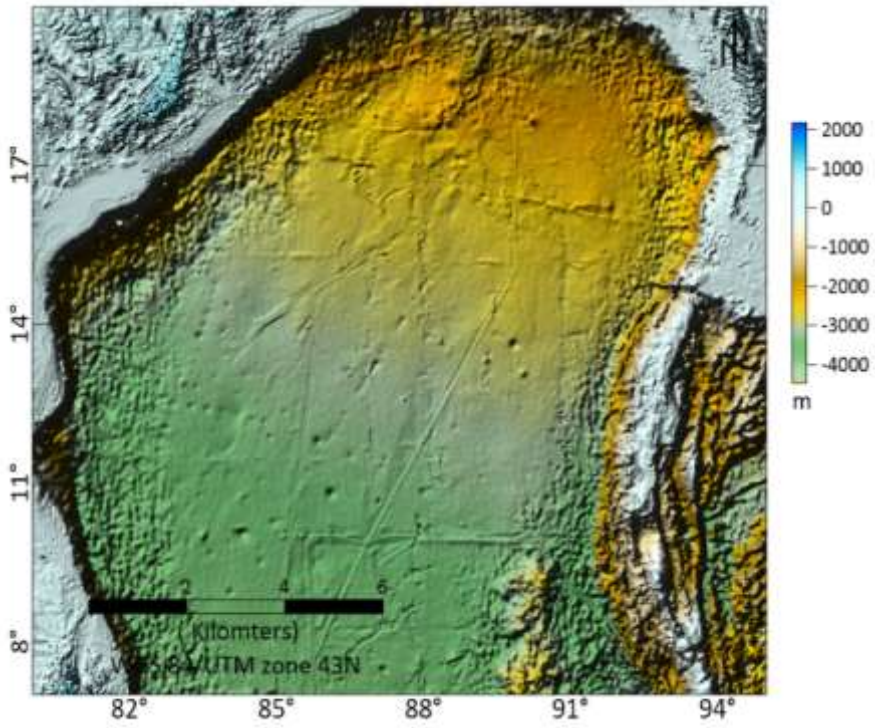

Figure 9: Sea floor age map in the Bay of Bengal

REDVET - Revista electrónica de Veterinaria - ISSN 1695-7504
Vol 25, No. 1 (2024)
http://www.veterinaria.org
Article Received: 12 Jan 2024, Revised: 28 Jan 2024, Accepted: 16 Feb 2024

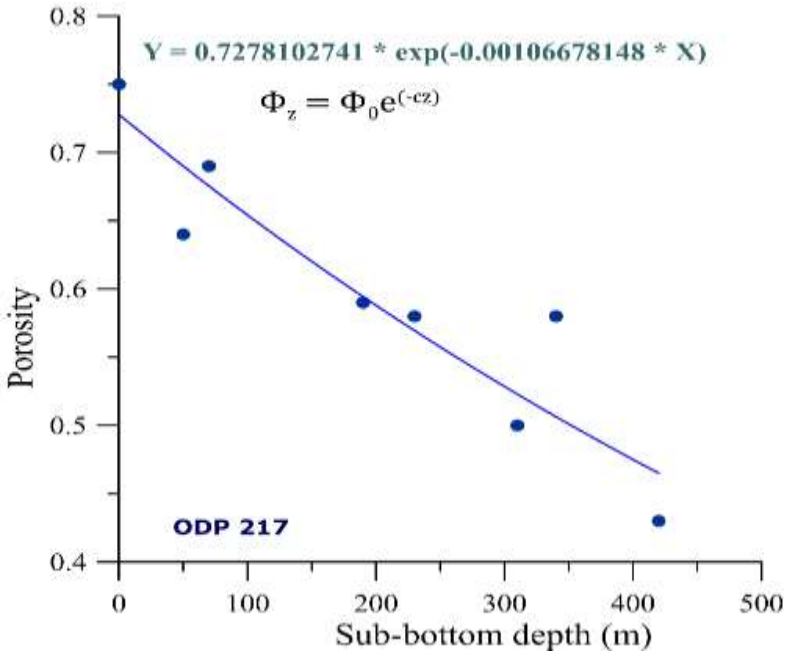

Figure 10: Porosity-depth plot of 217 ODP well (Vonder Botch et al., 1974).Dark blue straight line represents exponential fit to the plot

Equation (4) represents a three-dimensional grid with 5.5 km × 5.5 km of horizontal dimension and an average vertical spacing of 6 km. It determines the lithosphere's density owing to changes in thermal expansion and pressure. When it turns out that the mantle density, or ρ_0, at standard atmospheric pressure (P_0) and normal temperature (273K), is 3300 kgm^{-3}, the coefficient of thermal expansion, or α(T), is presumably 3.28 $X10^{-5}K^{-1}$ (Greenhalgh and Kusznir, 2007). In equation (3), here are two unknown parameters: the lithospheric thermal equilibrium period (t) and the lithospheric stretching factor (β), which is infinite for oceanic areas since most of the region under discussion is oceanic. The crustal age grid of Muller et al. (2008) oceanic is used to calculate the lithospheric thermal equilibrium time, or t. The lithospheric thermal equilibrium time, or t, is calculated using Oceanic's crustal age grid (Muller et al., 2008).

The thermal decay constant (τ) and depth to the base of the lithosphere (a) were measured by Ma and Dalton (2017), and their respective values were found to be 62.8 and 125 km. Based on an investigation of Rayleigh wave phase velocity maps for the northern Indian Ocean, Ma and Dalton (2017) concluded that the temperature at the base of the lithosphere (T_l) is 1450°C. Once the combined impacts of bathymetry, sediment, lithosphere, and pressure variations are removed, the Complete Bouguer Anomaly (CBA) gravity anomalies are eliminated, yielding the Mantle Residual Gravity Anomaly (MRGA) (Figure 11). After that, MRGA are inverted using equation (5), assuming a density contrast of 400 kg/m^3 and a mean Moho depth of 21 km at the start (average assumed using CRUST1.0 model and accessible seismic refraction data from the bordering regions). Figure 12 displays the Moho depths that were derived from the 3D inverted MRGA data. Figure 13 displays Moho depths included from L. Shang et al., 2022. Figure 14 displays a comparison plot of Moho depths calculated from the 3D inverted CBA, MRGA, and published seismic research of L. Shang et al., 2022. By subtracting the whole thickness of the bathymetry and sediments from the Moho topography, the crustal thickness map has been generated (Figure 15). Before inversion, the CBA and MRGA were exposed to cosine taper low pass filters with wave lengths ranging from 83.33 km to 150 km in order to eliminate the influence of shallow sources that occur inside the crust. This work used the pure shear model (McKenzie, 1978, McKenzie et al., 2005) to infer the temperature field of the lithosphere mantle, which is obtained using multiple parameter sets. These fluctuations in heat and pressure in the lithospheric layer create anomalies in gravity. The model parameters have been tested by shifting their values throughout a range of values from prior studies in other locations, as there are no measure quantities in the research location. The following values are used in different regions to infer the thermal gravity anomalies: a=125, T_1=1333 °C, and $\alpha(T)=3.28\times10^{-5}$ K^{-1} for the North Pacific (Parsons and Sclater, 1977); a=95 km, T_1=1450 °C, and $\alpha(T)=3.138\times10^{-5}$ K^{-1},T_1=1300 and τ=62.8 Ma for the North-eastern Atlantic region (Greenhalgh and Kusznir, 2007); a=95 km, T_1=1300 °C and $\alpha(T) = 2.55\times10^{-5}K^{-1}$ for eastern and South-eastern Asia (Li and Wang, 2016); a=125 km,T_1=1333 °C, τ=62.8Ma and $\alpha(T)=3.28\times10^{-5}$ K^{-1} for the South China Sea (Bai et al, 2014).

For the ongoing study attempt. According to Ma and Dalton's (2017) analysis, the Rayleigh wave phase velocity map for the northern Indian Ocean suggests that the lithosphere's thickness (a) is 125 m and its base temperature (T_1) is 1450°C. At 62.8 Ma and $3.28X10^{-5}K^{-1}$, respectively, are assumed to be the values of τ and α(T). Since the precise amounts of these

REDVET - Revista electrónica de Veterinaria - ISSN 1695-7504
Vol 25, No. 1 (2024)
http://www.veterinaria.org
Article Received: 12 Jan 2024, Revised: 28 Jan 2024, Accepted: 16 Feb 2024

factors are unknown, the range of these attributes has been taken into account. Two approaches were used to determine the Moho depths: (i) without sediments but with sediment thickness and temperature terms retained, and (ii) without sediments but with sediment temperature and pressure related parameters retained. In addition to these changes, the parameters used in the computation of the anomalies related to temperature and pressure in the lithosphere were also modified.

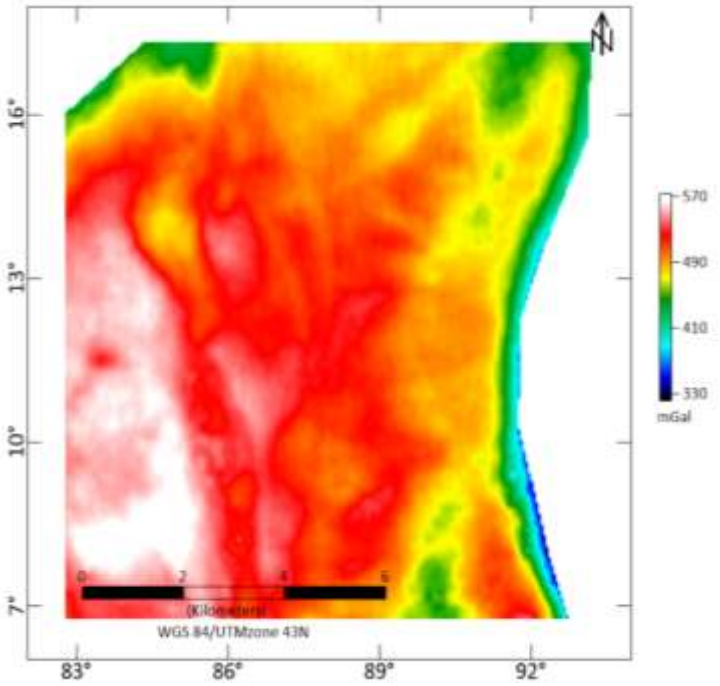

Figure 11: Mantle Residual Gravity Anomaly (MRGA) map after applying Bathymetry, Sediment, Temperature and Pressure corrections to Complete Bouguer Anomaly data

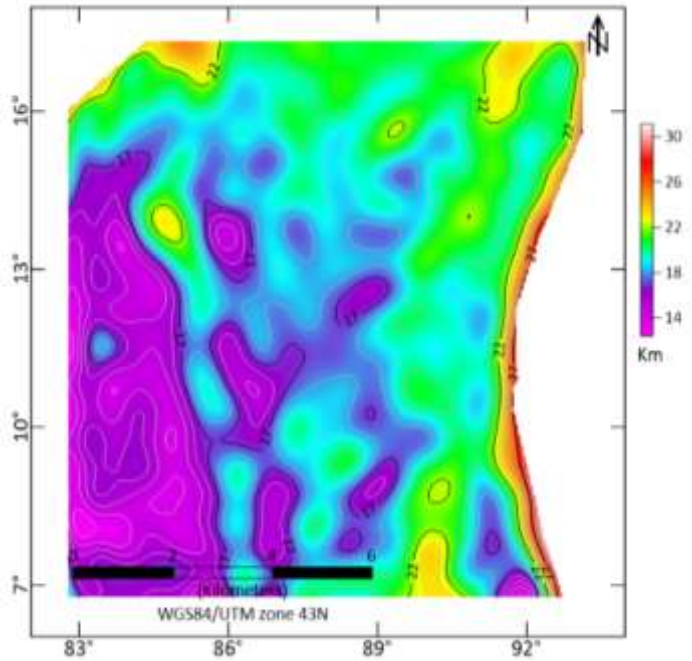

Figure 12: Moho depths variations obtained from the 3D inverted Mantle Residual Gravity Anomaly (MRGA).

REDVET - Revista electrónica de Veterinaria - ISSN 1695-7504
Vol 25, No. 1 (2024)
http://www.veterinaria.org
Article Received: 12 Jan 2024, Revised: 28 Jan 2024, Accepted: 16 Feb 2024

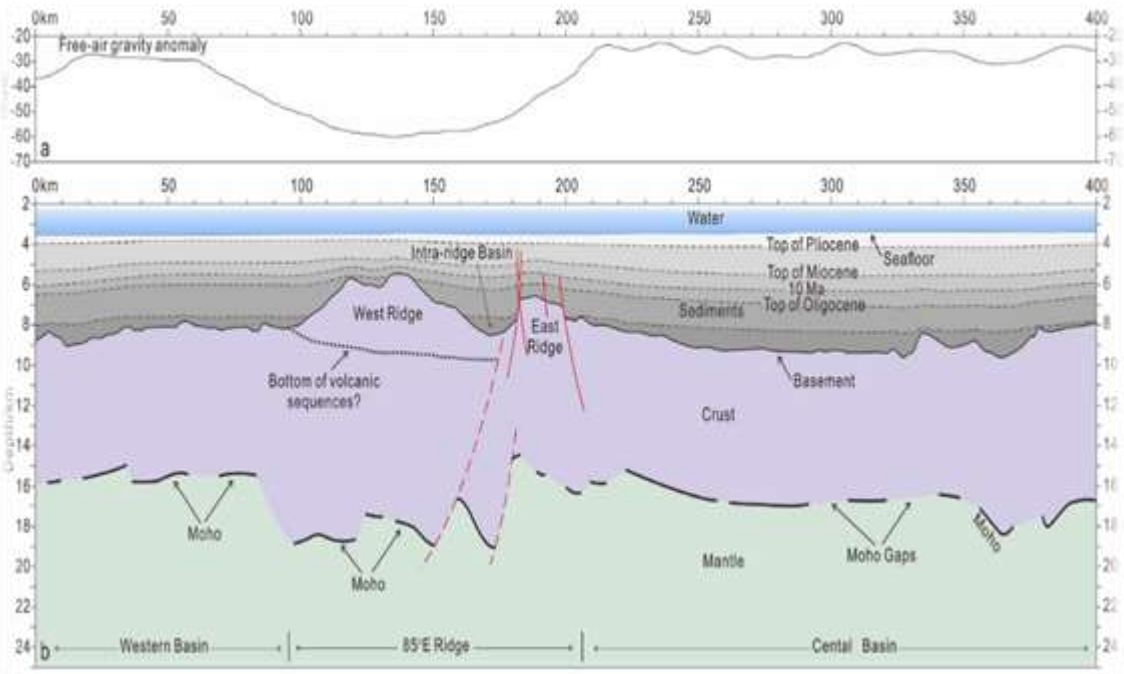

Figure 13: Moho depths plot have been incorporated from recent seismic studies of the L.Shang et al,.2022

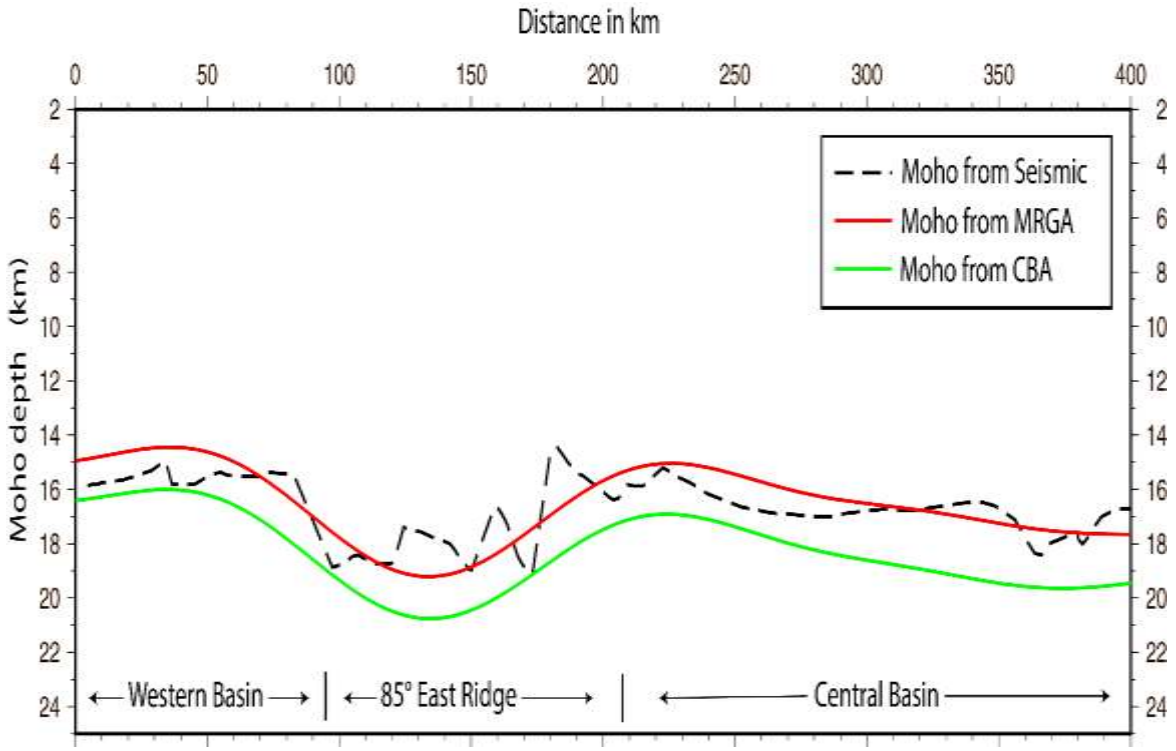

Figure 14: Comparison plot between the Moho depths obtained from the 3D inverted MRGA, that of CBA and that obtained from seismic results (from L.Shang et al, .2022)

REDVET - Revista electrónica de Veterinaria - ISSN 1695-7504
Vol 25, No. 1 (2024)
http://www.veterinaria.org
Article Received: 12 Jan 2024, Revised: 28 Jan 2024, Accepted: 16 Feb 2024

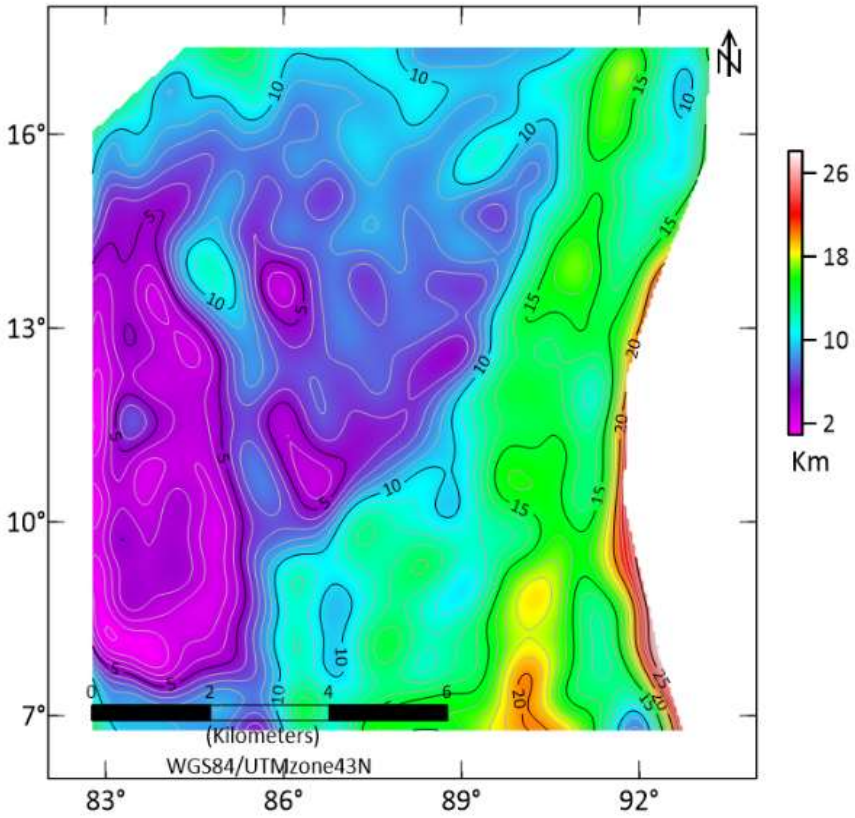

Figure 15: Crustal thickness produced by this study after applying the sediment, temperature, and pressure corrections to CBA

5. Data and Methodology

In the current investigation, high resolution satellite-derived free air gravity data (V.24.1, Sandwell and Smith, 2009; Sandwell et al., 2014) and bathymetry data (V.18.1, Smith and Sandwell, 1997) obtained from satellite altimetry, each with a resolution of one arc minute, were generated from re-tracked Seasat, Geosat GM, TOPEX/POSEIDON, ERS-1/2, Cryosat-2, and Jason-1 altimeter data (ftp:/topex.ucsd.edu/pub/ global grav 1min/) with a resolution of one arc minute. Smith and Sandwell (1997) state that the basic technique is to first filter gravity data to the mean sea floor depth, and then filter satellite gravity data in the 16–160 km wavelength range. Bathymetry from the National Geophysical Data Centre (NGDC) and bathymetry showed high coherency for wavelengths longer than 100 km (Smith and Sandwell, 1997). This suggests that bathymetry from later times is useful for studies up to the Moho undulations, providing information to short wavelengths greater than 20 km. Since the FAG data set offers information down to incredibly short wavelengths (less than 20 km), it is useful for in-depth, localised study. The research area is situated above the Indian Ocean Geoidal Low (IOGL), which is distinguished by extended spatial wave lengths that are assumed to originate in the Mantle (Kahle et al., 1978). Because current research is concentrated on the crust and upper mantle component up to Moho. The study area is located above the Indian Ocean Geoidal Low (IOGL), which is characterised by long spatial wave lengths thought to have its origin in the Mantle (Kahle et al., 1978). Because the focus of present research is on the upper mantle component up to Moho and the crust. To evaluate the long wave length gravity effect of IOGL, FAG data must be cleaned of longer wave length abnormalities resulting from deeper Mantle. The Geoid Data (http://icgem.gfz-potsdam.de, Barthelmes and Kohler, 2016) was used, and the spherical harmonic coefficient of EIGEN 6C4 (Forste et al., 2015) was removed from the FAG data up to degree and order of 50. Low pass filters matching spherical harmonic coefficient 50 (~800 Km) wave length were used, with coefficients of roll off between the degree 30-70 (~1333 Km – 571 Km) wavelengths, to avoid the ringing effect induced by the severe truncation at degree 50. The long wave length gravity anomalies that were extracted from the FAG anomaly were subtracted to create the FAG-IOGL map (V.24.1, Sandwell and Smith, 2009; Sandwell et al., 2014). (Figure 4).

The bathymetric strong gravity effect is part of the anomaly map produced by FAG-IOGL. Because the FAG map shows the correlation with the bathymetry, it becomes difficult to evaluate whether the reported anomaly is caused by seabed topography or a subsurface geological structure. The FAG-IOGL map approximates the bathymetry due to the sharp contrast in density between the sea floor and the underlying sediments. Bouguer reduction, which is primarily linked to variations in lateral density in the Moho and Crust topography, might be used to lessen this reliance on FAG-IOGL data.

REDVET - Revista electrónica de Veterinaria - ISSN 1695-7504
Vol 25, No. 1 (2024)
http://www.veterinaria.org
Article Received: 12 Jan 2024, Revised: 28 Jan 2024, Accepted: 16 Feb 2024

In the current research, the full Bouguer anomaly from FAG-IOGL has been computed using the FORTRAN software (Fullea et al., 2008) that computes the Bouguer plate, curvature, and terrain corrections. The primary inputs for this programme include of bathymetry data, seawater and crust densities, and gridded free air gravity data. In order to estimate the local topography, or bathymetry, the Bouguer plate correction, often referred to as Bullard A, uses a slab with an infinite lateral area, constant density, and thickness equal to the elevation of a site with respect to mean sea level. Furthermore, it is predicated on the infinite slab using the densities of seawater and crust (2900 kgm^{-3}) (1030kgm^{-3}). Bullard B (Curvature Correction): Up to a distance of 166.7 km, the Bouguer slab can be substituted by a spherical cap of the same thickness. The spherical cap has less of an effect than the infinite slab since the part of the slab that extends to infinity above Earth is shorter.

Nevertheless, the earth's curvature-induced sub-slab has a bigger impact than the slab itself. Latitude has no effect on the thickness or surface radius of the spherical cap. The spherical cap's curved shape, however, depends on latitude and central angle. (LaFehr.1991).The topography's effects above and below the computation location are included in Bullard C's correction for terrain (Nowell, 1999). It could be advantageous or disadvantageous for offshore locations. However, it only helps with Land points. The limit for the intermediate zone is 20 km, 2 km, and for the far zone it is 167 km, 4 km. When topographic reliefs are estimated, each grid point in the data is regarded as the flat top of a square prism, minimising their extreme effects (Fullea et al., 2008). Slab, curvature, and terrain correction can be used to create a complete Bouguer anomaly map (CBA) from the geoid corrected free air anomaly map (FAG-IOGL) (Figure 5)The geoid corrected free air anomaly map (FAG-IOGL) can be converted into a full Bouguer anomaly map (CBA) by combining slab, curvature, and terrain correction (Figure 5).

5.1 Moho depth estimation by inverting the Gravity data:

Onshore studies often make use of Bouguer anomalies, while offshore investigations favour free air anomalies. But these are used to show how the density of the bottom affects things and to keep bathymetry from going .By merging CBA with the gravity inversion, Moho undulations are ultimately produced. Nevertheless, the simple Bouguer anomaly is produced by the geoid corrected free air anomaly when bathymetry correction is the sole alteration that is carried out. g off track. Applying slab, curvature, terrain, and bathymetry corrections to the geoid corrected free air anomaly map (FAG-IOGL) yields the full Bouguer anomaly (CBA) (Figure 5). Total Bouguer anomaly removal of non-geological components of gravity anomalies enhancing subsurface mass fluctuations is the primary goal. To isolate the gravity anomalies only due to the Moho interface, it is crucial to remove all other contributions to CBA. A variety of modifications can be made to produce MRGA that shows the gravitational anomaly caused by the Moho Interface's geometry. Age, temperature, pressure, and sediment are the four variables that must be taken into account when adjusting the CBA. In other words, MRGA can only be achieved once the CBA has been isolated from the effects of the sedimentary layers' gravitational pull and from the temperature and pressure fluctuations within the lithospheric mantle (Figure 11). When gravity inversion and MRGA work together, they create Moho undulations. The text below explains these changes. Figure 16 shows a schematic flow that summarizes the study's work.

5.2 Gravity effect of sediments

Considering the correlation between sediment thickness, porosity, and density, studies have examined the gravitational effects of sediments with varied densities (Sawyer, 1985; Bai et al., 2014). The impact of sediment density can be determined by utilizing the correlation between the sediment's porosity ($\emptyset_z$) and the underlying sediment's thickness.

$$\emptyset_z = \emptyset_0 e^{-cz}, \quad (1)$$

Where c is a constant that has been determined empirically and has a unit of one divided by depth, and $\emptyset_0$ is the initial porosity. According to Sawyer (1985), the density (ρ_z) will be once the sedimentary pore space is filled with sea water, with z km of material above it.

$$\rho_z = \emptyset_z \rho_w + (1-\emptyset_z)\rho_{sg} \quad (2)$$

This equation has variables ρ_w (the density of water) and ρ_{sg} (the density of grains), ρ (the density of the slab), z_0 (the height of the viewing plane, with the sea surface at 0), and z_1 and z_2 (the depth to the top and bottom of the layer, respectively).

5.3. Gravity effect of Temperature and Pressure variations

It is in the oceanic zones that the lateral lithosphere oscillations-triggered lithosphere thermal gravity anomaly is most noticeable. According to Greenhalgh and Kusznir (2007), it decreases as it gets closer to the rifted continental margin, although it produces around -380mGal near oceanic ridges. The increased gradient of the oceanic lithosphere, which tends to anticipate Moho depths that are significantly bigger than actual depths, is the major cause of the enormous negative gravity anomaly component that requires lithospheric thermal gravity correction (Cowie and Kusznir, 2012). Lithospheric temperature calculations are necessary in order to determine the lithospheric thermal gravity anomaly. Next, we calculate

REDVET - Revista electrónica de Veterinaria - ISSN 1695-7504
Vol 25, No. 1 (2024)
http://www.veterinaria.org
Article Received: 12 Jan 2024, Revised: 28 Jan 2024, Accepted: 16 Feb 2024

and apply density perturbations that are caused by the anomaly, which is produced by oceanic Lithospheric cooling effects. A shear model is employed to build the lithospheric mantle temperature field at depth z, where z is the vertical distance between the target point and the model basement, as described by McKenzie (1978). The formula for this shear model is as

$$T_z=T_1\{1-\frac{z}{a}+\frac{2}{\pi}\sum_{n=1}^{\infty}\frac{(-1)^{n+1}}{n}[\frac{\beta}{n\pi}\sin\frac{n\pi}{\beta}]\times\exp(\frac{-n^2t}{\tau})\sin\frac{n\pi z}{a}\} \quad (3)$$

Where does T_1 represent the base of the lithosphere temperature?
"a" represents the model's base depth, and "τ" stands for the thermal decay constant of lithospheric cooling.

The crustal age is denoted by t, while β represents the stretching factors of the lithospheric crust.

In unstretched continental areas, the stretching factor (β) is one; in stretched continental areas, it is the ratio of the crustal thickness before stretching to the thickness being studied at the moment. It is comparable to the infinite stretching factor in the case of coastal locations. Most observed marine magnetic lineation can be utilized as a marker for the age of the oceanic crust when determining the thermal structure of the lithosphere using the plate cooling model (Bai et al., 2014). For this case, Muller et al. (2008) oceanic crustal age grid was utilized. To represent the changes in Lithospheric density caused by pressure compression due to overburden stress, the compressibility coefficient (γ_T) is utilized. This coefficient is inversely related to the pressure change at temperature T and the bulk modulus (K_T). Bulk moduli of rich upper mantle minerals, such as forsterite, can be estimated linearly with respect to temperature (Kroll et al., 2012).
KT = 127.97−0.0232 (T−300)

It is possible to compute the changes in the lithospheric mantle density brought on by pressure compression and thermal expansion utilizing

$$\rho_{TP}=\rho_o[1-\propto(T)(T-T_O)+\gamma_T[P(z)-P_o] \quad (4)$$

In this context, $\propto(T)$ represents the thermal expansion coefficient, ρ_o stands for the mantle density at temperature T_0, and P(z) denotes the pressure at the point where temperature T is equal to.

5.4. 3D-Gravity inversion

The code used in this study to estimate the three-dimensional geometry of the Moho interface from the gravity anomalies (Complete Bouguer Anomaly) was created by Gomez-Ortiz and Agarwal (2005) and is based on the wave number domain inversion technique (1974) established by Oldenburg. To obtain Mantle Residual Gravity Anomalies (MRGA) (CBA), the Geoid corrected Free Air Anomaly is subjected to Bullard (A), Bullard (B), and Bullard (C) corrections. By applying the bathymetry, sediment, temperature, and pressure corrections to CBA data, MRGA is generated.

$$F\,[h(x,y)]=-\frac{F[\Delta g(x,y)e^{|k|z}}{2\pi G\rho}-\sum_{n=2}^{\infty}\frac{|k|^{n-1}}{n!}F[h^n(x,y)] \quad (5)$$

The variable ρ represents the interface density, G stands for the universal gravitational constant, h(x, y) is the interface depth, Δg(x, y) is the gridded gravity anomaly, z is the mean depth of the horizontal interface, and is $|k|^{n-1}$the absolute value of the wave vector. The Moho surface's topography was computed using an iterative technique (Chappell and Kusznir, 2008; Bai et al., 2014). There has been an application of a cosine low pass filter to both the MRGA and the CBA in order to guarantee that the equation that was discussed earlier will converge before the beginning of the gravity inversion process. In order to remove short-wavelength components, this filter is applied to data generated by shallower sources deep under the earth's surface. Also, the consistent densities of the crust and mantle are necessary for the uniqueness theorem of Smith (1961).

REDVET - Revista electrónica de Veterinaria - ISSN 1695-7504
Vol 25, No. 1 (2024)
http://www.veterinaria.org
Article Received: 12 Jan 2024, Revised: 28 Jan 2024, Accepted: 16 Feb 2024

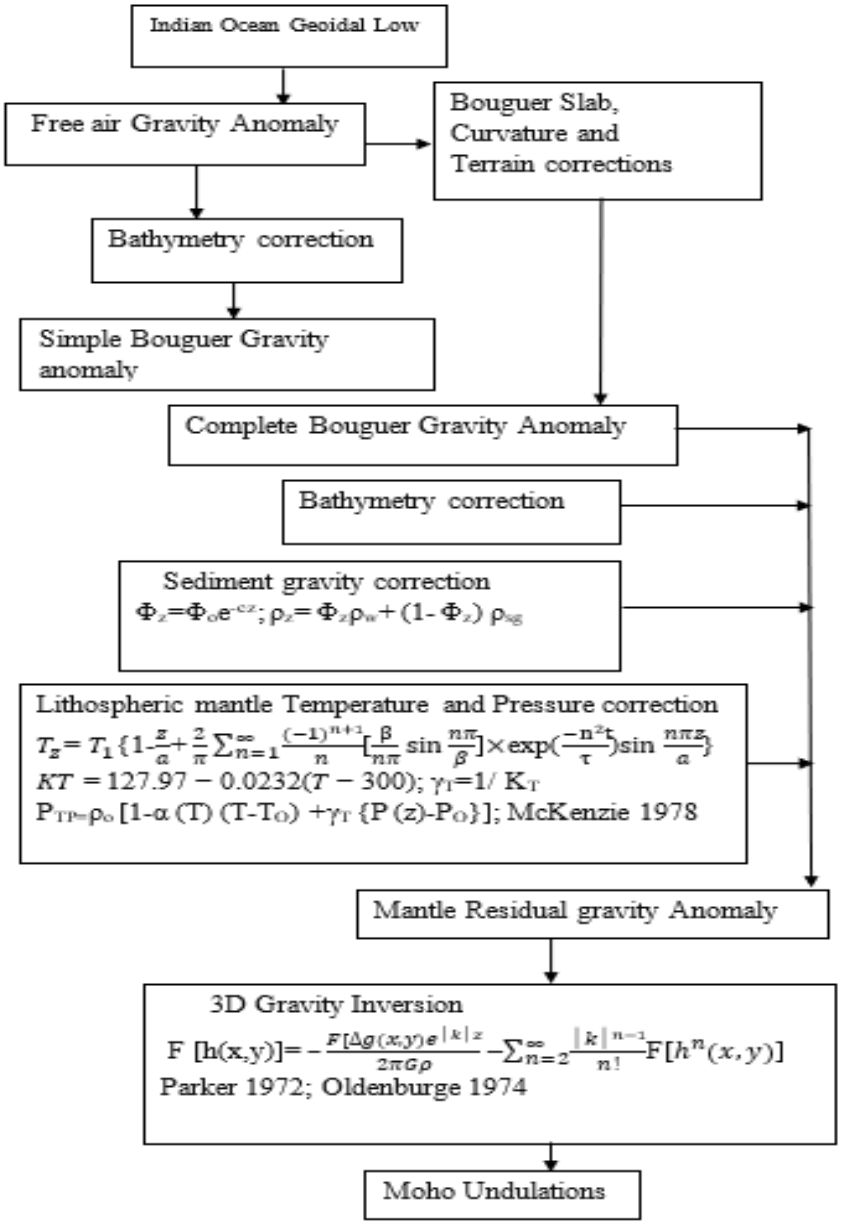

Figure16: A schematic flow with summarizing the work undertaken in the present study is shown

6. Results and Discussions

In this investigation, bathymetry, sediment, and lithospheric heat and pressure corrections have been made to the MRGA in order for figuring out Moho undulations beneath the 85°E and 90°E ridges and their surrounding areas. The MRGA inversion yielded estimated Moho depths ranging from 14 to 30 km. The thickness of the crust varies from 2 to 26 km. The estimated Moho depths range from 10 to 28 km by inverting CBA and not utilising bathymetry, sediment, thermal, or pressure corrections. Based on the inversion of both the CBA and MRGA from the current research, the mean depths to the Moho interface are calculated to be 19 km and 22 km respective. These are shallower than both the Moho interface (~23 km) calculated using inverted gravity data by Radhakrishna et al. (2010) and the Moho interface (23 km) derived from the examination of Rayleigh wave group velocity dispersion data by Mitra et al. (2011). Furthermore, the Moho computed (26.6 km) using spectral analysis of 108 Overlapping (50 percent) widows of each dimension 230 km, and the mean depths to Moho (25 km) were computed from our prior investigations employing RAPS of FAG data. The depths to Moho, which are the results of using MRGA (17(±5) Km, 15.5(±3.5) Km, and 20(±2) Km, and 15.5(±3.5) Km, 20(±1) Km, and 23(±2) Km using CBA, in the Southern, Central, and Northern Bay of Bengal, are almost identical to the top of Moho Interface (17(± 3) Km, 20(±3) Km, and 30(±3) Km, respectively) by Mitra et al., 2011, using the analysis of the Rayleigh wave group velocity dispersion data, and that to Moho 10.5(±0.5) Km, 13.5(±2.5) Km, and 17(±1) Km) by the

Geoid and Gravity data 2D modelling studies of G.S. Rao et al., 2016. It has been noted that the crust's thickness varies, ranging from 13(±3) Km in the southern region to 5(±3) Km in the central region and 10(±2) Km in the northern BoB. (Fig. 15).

The depths to Moho that have been estimated (16 km & 19 km) from the current study using the MRGA and CBA, respectively, at the location of the DSDP hole 217 (location 9°N & 89°E) (Figure 2) are comparable to those that we previously investigated using FAG data and RAPS. At the seismic refraction station 270 (15.5°N & 90°E) (Figure 2), the Moho depth of 11.6 km, obtained by Naini and Layden in 1973 (where velocity changes from 5.06 km/s to 6.28 km/s), and that of 14.3 km, towards the east of 88°E, computed from our previous studies using Radially averaged power spectrum of Free air gravity data, are found to be shallower than that of 21 km using CBA and 19 km using MRGA computed from the present studies. These measurements are closely resemble the 19 km computed from 3D inversion studies of Radhakrishna et al., 2010. Beneath this refraction station in the centre BoB is a 9 km thick crust (Figure 15). Moho is located at a depth of 14 km at the position of DSDP well 218 (8°N & 86.3°E) (Figure 2) in the southernmost BoB, according to seismic investigations conducted in 1982 by Curray et al. using the GSZ method and seismic studies conducted in 1973 by Authors of Naini and Leyden using seism acoustic radio beacon (R/B 264). Using current 3D gravity inversion research, we have determined the depth to the Moho interface at the same location to be 19 km from the CBA and 19 km from the MRGA, respectively. The Moho depth is 15 km below, with a 5 km variation, based on 3D gravity inversion studies conducted by Radhakrishna et al in 2010. The results of the current investigation are similar to those published by Naini and Leyden (1973), Radhakrishna et al. (2010), and Curray et al. (1982).

Seismic investigation by L. Shang et al. (2022) indicates that the Moho depth in the Bay of Bengal is 17(±2) Km over the 400 km long Seismic profile MCS-1, which extends from 84°E to 88°E (at latitude 11°N) (Figure 2). Radhakrishna et al. (2010) used 3D gravity inversion modelling to measure the Moho depth, which came out to be approximately 19(±3) km. The 2D gravity modelling work by L. Shang et al. (2022) calculated the Moho depth to be 16.5(±1.5) km. Research by Radhakrishna et al. (2010) using 3D gravity inversion tests in the Bay of Bengal shows that the Moho depth fluctuates by about 18(±4) Km. In our current 3D gravity inversion research, we have determined the Moho depths to be 18(±3) Km and 16.5(±2.5) Km, respectively, using CBA and MRGA. The Moho depth values obtained from this analysis are more in line with previous research along this seismic profile by L. Shang et al., 2022, and Radhakrishna et al., 2010.

The Moho depth under 85°E is around 16.5 km (±1.5 km) (~10-11 s TWT), in the central basin is about 15 km (~10s TWT), and in the western basin is about 15 km (~10s TWT), according to the authors of L. Shang et al., 2022, based on seismic reflection data. Gravity's modelling research by L. Shang et al. from 2022 states that the Moho depth in the western basin is 15(±0.5) Km, the Moho depth below the 85°E Ridge is 17.5(±1.5) Km, and the Moho depth in the central basin is 16.5(±1.5) Km. Based on our current 3D inversion research using CBA & MRGA, we have determined the Moho depth in the western basin to be 17.5(±1.5) Km & 15.5(±1.5) Km, that under the 85°E Ridge to be 19.5(±1.5) Km & 17(±2) Km, and that in the central basin to be 18.5(±1.5) Km & 16.5(±1.5) Km. The Bay of Bengal study's findings are consistent with the seismic reflection analysis and gravity modelling study by L. Shang et al. 2022. These patterns indicate a 2–10 km variation in crustal thickness from west to east (Figure 15).

Conclusions

Moho depths and Crustal thickness have been determined for CBA and MRGA using the 3D inversion. The Moho depths in the oceanic zones exhibit a notable enhancement when the pressure and temperature corrections are included to the calculations made using the MRGA. Moho depths from CBA and MRGA are 10 km to 26 km and 14 km to 30 km, respectively, throughout the entire investigation region. A 2 to 28 km variance in crustal thickness is present over the whole studied region. The Moho depth values obtained by L. Shang et al. (2022) in the western basin are in good agreement with the Moho estimated using CBA and MRGA, which vary between around 17.5 (±1.5) Km and 16 (±1) Km. The northern region's thicker crust could be the product of magmatic underplating of the oceanic crust or reworked stretched continental crust. The thickness of the crust beneath the 85˚E Ridge varies between 2 and 7 km in the western and central BoB, and between 10 and 18 km in the eastern BoB. Moho depth ranges from 25 km north to 18 km south using CBA and 23 km north to 19 km south using MRGA.

Acknowledgement

The writers are grateful to Andhra University, Visakhapatnam, for their continuous encouragement and assistance, as well as for giving them permission to publish this work. The authors thank Andhra University in Visakhapatnam, India, for their help and for hosting this work. Free-air gravity data was collected from TOPEX (ftp:/topex.ucsd.edu/pub/global grav 1min/). The editors-in-chief are greatly regarded by the authors.

Conflict of interest: No conflicts of interest are disclosed by the authors.

References

1. Smith, R.A., 1961.A uniqueness theorem concerning gravity fields. Math. Proc. Cambridge Philos. Soc. 57,865.
2. Smith, W.H., Sandwell, D., 1997. Global sea floor topography from satellite altimetry and ship depth soundings. Science 277, 1956–1962.

3. Sreejith, K.M., Rajesh, S., Majumdhar, T.J., Rao, G.S., Radhakrishna, M., Krishna, K.S. and Rajawat Ajay, K.K., Chaubey, A.K., Krishna, K.S., Rao, D.G., Sar, D., 2010. Seaward dipping reflectors along SW continental margin of India: evidence for volcanic passive margin. Journal of Earth System Science 119, 803–813.
4. Anand, S.P., Rajaram, M., Majumdhar, T.J. and Bhattacharyya, R., 2009, Structure and Tectonics of 85°E Ridge from analysis of Geopotential data. Tectonophysics, v. 478, pp. 100-110.
5. Bai, Y., Williams, S.E., Muller, R.D., Liu, Z. Hosseinpour, M., 2014.Mapping crustal thickness using marine gravity data: methods and uncertainties. Geophysics79, G27– G36.
6. Baksi, A. K., T. R. Barmann, D. K. Paul, and E. Farrar (1987), Widespread early Cretaceous flood basalt volcanism in eastern India: Geochemical data from Rajmahal-Bengal-Sylhet Traps, Chem. Geol., 63, 133–141, doi:10.1016/0009-2541(87)90080-5.
7. Barthelmes, F., Köhler, W., 2016. International Centre for Global Earth Models (ICGEM), in: Drewes, H., Kuglitsch, F., Adám, J. et al. (Eds.), the Geodesists Handbook 2016, J. Geodesy. vol. 90, pp. 907–1205
8. Bansal. A.R., Fair head, Green .C.M &, Fletcher. K.M.U. Revised gravity offshore India and Isostatic compensation of sub marine features. Tectonophysics (404) (2005)1-22.
9. Chappell, A.R., Kusznir, N.J., 2008. Three-dimensional gravity inversion for Moho depth at rifted continental margins incorporating a lithosphere thermal gravity anomaly correction. Geophys. J. Int. 174, 1–13.
10. Cowie, L., Kusznir. 2012. Mapping crustal thickness and Oceanic lithosphere distribution in Eastern Mediterranean using gravity inversion. Pet. Geosci. 18, 373–380.
11. Corchete.V.2017.S-velocity characterization of the crust and upper mantle structure beneath Bay of Bengal. Geological Journal. 2018; 1–10. DOI: 10.1002/gj.3139. Curray, J.R., Moore, D.G., 1971. Growth of Bengal Deep-Sea Fan and Denudation in the Himalayas. Geol. Soc. Am. Bull. 82, 563–572.
12. Cowie, L., Kusznir. 2012. Mapping crustal thickness and Oceanic lithosphere distribution in Eastern Mediterranean using gravity inversion. Pet. Geosci. 18, 373–380.
13. Curray, J. R and Moore.D.G.1974.Sedimentary and Tectonic process in the Bengal Fan Deep Sea In; Geosynclines. Burke. C.A and Drake C.L. (Eds). Geology of Continental Margins. Springer-Verlag. New York. pp. 617-627.
14. Desa, M.A., Ramana, M.V., Ramprasad, T., Anuradha, M., Lall, M.V., Kumar, B.J.P., 2013. Geophysical signatures over and around the northern segment of the 85◦E Ridge,
15. Fullea, J., Fernàndez, M., Zeyen, H., 2008. FA2BOUG-A FORTRAN 90 code to compute Bouguer gravity anomalies from gridded free-air anomalies: Application to the Atlantic-Mediterranean transition zone. Comput. Geosci. 34, 1665–1681.
16. Forste, C., Bruinsma, S., Abrikosov, O., Lemoine, J.M., Marty, J.C., Flechtner, F., Balmino, G., Barthelmes, F., Biancale, R., 2015. EIGEN-6C4, the latest combined global gravity field model including GOCE data up to degree and order 2190 of GFZ Potsdam and GRGS Toulouse. GFZ Data Services
17. Gibbons, A.D., Whittaker, J.M. and Muller, R.D., 2013, the breakup of East Gondwana: Assimilating constraints from Cretaceous ocean basins around India into a best-fit tectonic model. Journal of Geophysical Research-Solid Earth, v. 118, pp. 808-822.
18. Gomez-Ortiz, D., Agarwal, B.N.P., 2005.3 DINVER.M: A MATLAB program to invert the gravity anomaly over a 3D horizontal density interface by Parker-Oldenburg's algorithm. Comput. Geosci.31, 513–520.
19. GopalaRao, D., Krishna, K.S., Sar, D., 1997.Crustal evolution and sedimentation history of the Bay of Bengal since the cretaceous. J. Geophys. Res. Solid Earth 102 (B8), 17,747–17,768.
20. Green halgh, E.E. Kushner, N.J., Evidence for thin oceanic crust on the extinct Aegir Ridge, Norwegian Basin, NE Atlantic derived from satellite gravity inversion. Geophys. Res. Lett. 34, L06305.
21. Homrighausen, S., Hoernle, K., Wartho, J.A., Hauff, F., Werner, R., 2021. Do the 85◦E Ridge and Conrad rise form a hotspot track crossing the Indian Ocean? Lithos 398- 399, 206234.
22. Kahle, H.G., Chapman, M., Talwani, M., 1978. Detailed 1×1 gravimetric Indian Ocean Geoid and comparison with Geos-3 radar altimeter geoid profiles. Geophys. J. R. Astron. Soc. 55, 703–720
23. Krishna, K.S., Michael, L., Bhattacharyya, R., Mujumdar, T.J., 2009. Geoid and gravity anomaly data of conjugate regions of Bay of Bengal and Enderby Basin: New constraints on breakup and early spreading history between India and Antarctica. J. Geophys. Res. Solid Earth 114 (B03102), 1–21.
24. Krishna, K.S., Bull, J.M., Ishizuka, O., Scruton, R.A., Jaishankar, S. and Banakar, V.K., 2014. Growth of the Afanasy Nikitin seamount and its relationship with the 85°E Ridge, northeastern Indian Ocean. Journal of Earth System Science, v. 123, pp. 33-47.
25. Krishna, K. S., Ismaiel, M., Srinivas, K., GopalaRao, D., Mishra, J and Saha, D., Sediment pathways and emergence of Himalayan source material in the Bay of Bengal. Current Science, 2016, 110.
26. Kroll, H., Kirfel, A., Heinemann, R., Barbier, B., 2012. Volume thermal expansion and related thermo physical parameters in the Mg, Fe olivine solid-solution series. Eur. J. Mineral. 24, 935–956.
27. K.S. Krishna. Structure and evolution of the Afanasy Nikitin seamount, buried hills and 85°E Ridge in the northeastern Indian Ocean. Earth and Planetary Science Letters 209 (2003) 379-394.
28. Kumar, R.T.R., Windley, B.F., 2013. Spatial variations of effective elastic thickness over the Ninety East Ridge and implications for its structure and tectonic evolution. Tectonophysics 608, 847–856.

29. Kunnummal P Anand. S.P.2019.Qualitative appraisal of high-resolution satellite derived free air gravity anomalies over the Maldive Ridge and adjoining ocean basins, western Indian Ocean. Journal of Asian Earth Sciences 169 (2019) 199–209.
30. Laske, G., Masters, G., Ma, Z., Pasyanos, M., 2013. Update on CRUST1.0 – A 1-degree Global Model of Earth's Crust. In: EGU General Assembly Conference Abstracts 15, p. 2658.
31. Luning Shang, Gang Hu, Jun Pan, Peter D. Clift, Hailong Li, Yong Zhang, Chuansheng Yang, HaoWu, Weimin Ran.2022, Hotspot volcanism along a leaky fracture zone contributes the formation of the 85◦E Ridge at 11°N latitude, Bay of Bengal. Tectonophysics 837 (2022) 229453. https://doi.org/10.1016/j.tecto.2022.229453
32. McKenzie, D., Jackson, J., Priestley, K., 2005. Thermal structure of oceanic and continental lithosphere. Earth Planet. Sci. Lett. 233, 337–349.
33. McKenzie, D.P., 1978. Some remarks on the development of sedimentary Basins. Earth Planet. Sci. Lett. 40, 25–32.
34. Mishra, D., 1991. Magnetic crust in the Bay of Bengal. Mar. Geol. 99, 257–261.https:// doi.org/10.1016/0025-3227 (91)90095-L.
35. Michael, L. & Krishna, K.S., 2011. Dating of the 85◦E Ridge (northeastern Indian Ocean)
36. Muller, R.D., Sdrolias, M., Gaina, C., Roest, W.R., 2008. Age, spreading rates, and spreading asymmetry of the world's ocean crust. Geochem. Geophys. Geosyst. 9, Q04006.
37. Oldenburg, D.W., 1974. The inversion and interpretation of gravity anomalies. Geophysics 34, 526–536
38. Parker, R.L., 1972. The rapid calculation of potential anomalies. Geophys. J. R. Astron. Soc. 31, 447–455.
39. Parsons, B. & Sclater, J.G., 1977. An analysis of the variation of ocean floor bathymetry and heat flow with age, J. Geophys. Res., 82, 803–827.
40. Pringle, M. S., F. A. Frey, and E. M. Mervine (2008), A simple linear age progression for the Ninety east Ridge, Indian Ocean: New constraints on Indian plate motion and hotspot dynamics, EOS, Trans. AGU, 89 (53) Fall Mtg. Suppl., abstract T54B-03.
41. Radhakrishna, M., Srinivasa, R.G., Nayak, S., Bastia, R., Twinkle, D., 2012. Early Cretaceous fracture zones in the Bay of Bengal and their tectonic implications: Constraints from multi-channel seismic reflection and potential field data. Tectonophysics 522-523, 187–197.
42. Radhakrishna, M., Subrahmanyam, C. and Twinkled.2010. Thin crust below Bay of Bengal inferred from 3-D gravity interpretation. Tectonophysics, 499, 93–10.
43. Ramana, M.V., Krishna, K.S., Ramprasad, T., Desa, M., Subrahmanyam, V., Sarma, K.V.L.N.S., 2001. Structure and tectonic evolution of the northeastern Indian ocean. In: Sen Gupta, R., Desa, E. (Eds.), the Indian Ocean a Perspective, vol. 2. Publ. Oxford and IBH publishing Co Pvt Ltd, New Delhi, pp. 731–816.
44. Sager, W. W., J. M. Bull, and K. S. Krishna (2013), Active faulting on the Ninety east Ridge and its relation to deformation of the Indo-Australian Plate, J. Geophys. Res. Solid Earth, 118, 4648–4668, doi: 10.1002 / jgrb.50319.
45. Shemenda, A.I., 1992. Horizontal lithosphere compression and subduction: constraints provided by physical modeling. J. Geophys. Res. 97, 11,097–11,116.
46. Sandwell, D.T. & McKenzie, K.R., 1989. Geoid height versus topography for oceanic plateaus and swells, J. Geophys. Res., 94, 7403–7418.
47. Sandwell, D.T., Smith, W.H.F., 2009. Global marine gravity from retracked Geosat and ERS-1 altimetry: ridge segmentation versus spreading rate. J. Geophys. Res. 114, B01411
48. Sandwell, D.T., Müller, R.D., Smith, W.H.F., Garcia, E., Francis, R., 2014. New global marine gravity model from CryoSat-2 and Jason-1 reveals buried tectonic structure. Science 346, 65–67
49. Sawyer, D.S., 1985.Total tectonic subsidence: a parameter for distinguishing crust type at the U.S. Atlantic Continental Margin. J. Geophys. Res. Solid Earth 90, 7751–7769.
50. Sclater. J. G and Fisher.R.L.1974.Evolution and East Central Indian Ocean with emphasis on the Tectonic settings of the Ninety East Ridge, Geol. Soc. Am. Bull.86.683-703.
51. , A.S., 2013, High-resolution residual geoid and gravity anomaly data of the northern Indian Ocean - an input to geological understanding. Journal of Asian Earth Science, v. 62, pp. 616-626.
52. Srinivasarao Manchala and S.K. Begum (2021). Characterization of density interfaces in the Bay of Bengal from high-resolution satellite-derived free-air gravity data .J. Ind. Geophys. Union, 25(6) (2021), 12-27.
53. Stein, C., Stein, S., 1992. A model for the global variation in oceanic depth and heat flow with lithospheric age. Nature 359, 123–128.
54. Subrahmanyam, V., Krishna, K.S., Radhakrishna Murthy, I.V., Sarma, K.V.L.N.S., Desa, Ramana, M.V., Kamesh Raju, K.A., 2001. Gravity anomalies and crustal structure of the Bay of Bengal. Earth Planet. Sci. Lett. 192, 447–456.
55. Whittaker, J.M., Goncharov, A., Williams, S.E., Müller, R.D., Leitchenkov, G., 2013. Global sediment thickness data set updated for the Australian-Antarctic Southern Ocean. Geochem. Geophys. Geosyst. 14, 3297–3305
56. Weis, D., and Frey, F. A., 1991, Isotope geochemistry of Ninety east Ridge basement basalts: SR, ND, and PB evidence for involvement of the Kerguelen hotspot, Proc. ODP, Sci. Results, College Station, Texas, Ocean Drilling Program 121, 591–610.
57. V. K. Illarionov O. Yu. Ganzha, D. A. Ilyinsky, V. Yu. Barmen, A. N. Boyko K. A. Roginskiy and A. Yu. Borisova. Nature of the Crust in the Southern Part of the Bay of Bengal and the Adjacent Part of the Central Basin (Indian

Ocean). Izvestiya.Atmospheric and Oceanic Physics, 2022, Vol. 58, No. 10, pp. 1289–1311. DOI: 10.1134/S0001433822100048.
58. Vonder Botch, C.C. et al., 1974. Site 214. Initial. Rep. Deep Sea Drill. Proj, 119-191.